Origin of nonhydrogenic hole transition in boron-doped silicon: An STM/S study

So-Dam Sohn●, Ja-Yong Koo, and Daejin Eom ●*

Korea Research Institute of Standards and Science, Yuseong, Daejeon 34113, Republic of Korea

The origin of the nonhydrogenic hole transition at ∼23 meV in the boron-doped silicon is still under debate. Here we employ the scanning tunneling microscope to uncover that a boron-containing complex on the silicon (111) surface shows three shallow acceptor states. Among them, the first excited state has the typical energy of the nonhydrogenic hole transition. We then show that this energy gap originates from the strain-induced mixing of the valence bands, unraveling a distinct origin for the nonhydrogenic hole transition in the boron-doped silicon.

I. INTRODUCTION

Shallow acceptor states in silicon (Si) attract renewed interest due to their potential applications in the solid-state quantum technology [1,2] and the terahertz laser field [3,4]. These states are normally described as the hydrogenic levels of the hole carrier moving in the uniform medium of a semiconductor with an effective mass m^* under the impurity potential [5]. Boron (B), which is the most important acceptor impurity in the Si technology, has the fourfold degenerate ground level ($1\Gamma_8^+$) with the binding energy of 44 meV and first excited hydrogenic level ($1\Gamma_8^-$) about 30 meV above the ground level [5,6]. Interestingly, some Raman [7–9] and infrared [10] spectroscopy measurements on the B-doped Si reveal the intriguing transition feature at ∼23 meV, implying the existence of a nonhydrogenic shallow state between the $1\Gamma_8^+$ and $1\Gamma_8^-$ levels of the B acceptor. Wright and Moonradian [7] ascribed it to the even-parity excited state ($1\Gamma_7^+$) of the B acceptor associated with the spin-orbit split-off band of Si [5,6,10,11]. Pavlov *et al.* [3], however, questions this assignment, arguing that the $1\Gamma_7^+$ state does not lie ∼23 meV above the $1\Gamma_8^+$ ground state, not even in the Si band gap. Instead, he suggests that it may be an odd-parity excited state of the B-containing complex like the so-called B-X center [12,13], not B itself, because the infrared detection of the absorption feature at ∼23 meV is enabled by the dipole-allowed transition [10]. This debate implies that the nonhydrogenic hole transition in B-doped Si has not reached complete understanding yet, leaving other possibilities open for its origin. It will thus be worthwhile to examine the diverse entities with the nonhydrogenic acceptor states not only in the bulk but also close to the surface region [14–19] for the identification of other possible origins.

Here we employ the scanning tunneling microscope (STM) to explore individual defects on the heavily B-doped Si(111) surface produced during the thermal annealing process. We find that a specific kind of defect involves shallow acceptor states as a consequence of the strain-induced mixing of the valence bands and that the energy spacing between the ground state and the lowest-lying excited one is ∼22 meV, providing

a strain-driven mechanism for the nonhydrogenic hole transition in the B-doped Si that differs from the $1\Gamma_7^+$ level of Wright and Moonradian [7] and also contrasts to the energy model assumed by Pavlov *et al.* [3,12].

II. EXPERIMENT

Our experiments were carried out using a low-temperature STM in the ultrahigh-vacuum chamber, whose base pressure was below 1×10^{-10} Torr. A heavily B-doped crystalline Si with the (111) orientation and the resistivity of <0.01 Ω cm was cleaned *in situ* by the repeated thermal flashes at ∼1370 K. It was then cooled down to room temperature at the rate of ∼2 K/s after the last flash. After that, it was quenched down to ∼4.5 K for the STM measurements. The STM probe tip was made of the Pt-Ir alloy. Also the Savitzky-Golay filter [20] was utilized to get the derivative part of the tunneling current spectra by digital differentiation.

III. RESULTS AND DISCUSSION

Shown in Fig. 1(a) is a typical STM topography of the heavily B-doped Si(111) surface with the $\sqrt{3} \times \sqrt{3}$ reconstruction whose lattice parameter is 0.67 nm [21]. Its structural model is displayed in Fig. 1(b) where the B atom occupies one-third of the third-layer sites (S_5 site) and the topmost Si adatom is sitting directly above the B atom (T_4 site) [22,23]. This $\sqrt{3} \times \sqrt{3}$ surface often contains two kinds of defects which are produced during an *in situ* thermal annealing process. One is the bright defect like the one indicated by the dotted arrow in Fig. 1(a), whose structure is well understood now; that is, a Si atom substitutes a B atom at the S_5 site to leave a dangling bond (DB) at the T_4 site as illustrated in Fig. 1(c) [24–27]. The other one is the dark defect like the one enclosed by the white rectangle in Fig. 1(a). This defect has been barely studied so far with its structure unknown. We term this defect as the D_A center in this paper and will show that it involves shallow acceptor states as does a B acceptor.

Figure 2(a) compares the electronic structure of the D_A center with that of the normal $\sqrt{3} \times \sqrt{3}$ surface. The latter (blue curve) develops no energy state within the Si band gap because the DB orbital of the Si adatom is passivated by the underlying B atom [28,29]. The former (red curve) also has
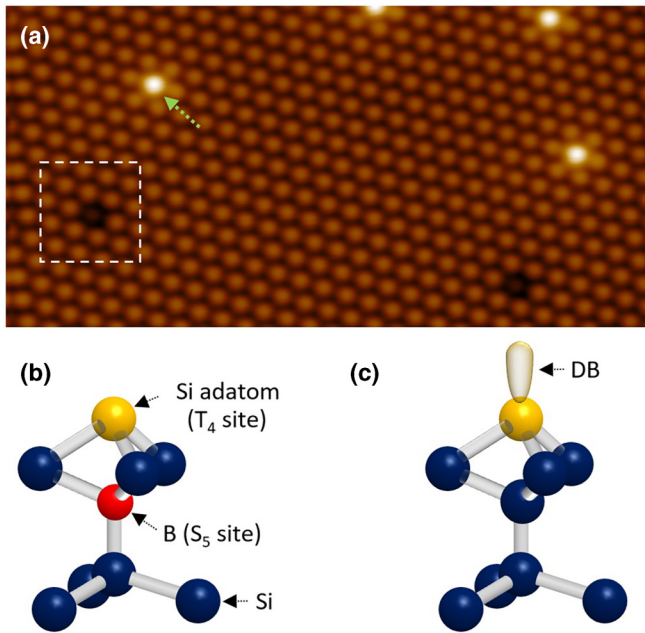
*d.eom@kriss.re.kr

FIG. 1. (a) Topography of heavily boron-doped Si(111) surface, whose lateral dimension is 20×10 nm^2. It is probed with the sample bias (V_{sample}) of $+2.0$ V and the tunneling current (I_t) of 1.0 nA. A bright (dark) defect is indicated by the arrow (white rectangle). (b), (c) Structural models of (b) the intact surface and (c) the bright defect.

FIG. 2. (a) Tunneling conductance (dI/dV) spectra probed at the normal $\sqrt{3} \times \sqrt{3}$ surface (blue curve) and at the D$_A$ center (red curve) with the bin spacing of 17 mV. (b)–(d) Bias-dependent topographies of the white rectangular region in Fig. 1(a) probed with $V_{\text{sample}} = -0.8$ V, -0.2 V, and $+2.5$ V, respectively, and $I_t = 1.0$ nA.

similar electronic structures as the latter (blue curve) only with slight changes near the valence band maximum (VBM): it does not produce any spectral feature in the middle of the band gap either, implying that the D$_A$ center does not contain the unpassivated DB orbital. The filled-state topography of the D$_A$ center around $V_{\text{sample}} = -0.2$ V displays three ball-like features in an equilateral triangle as shown in Fig. 2(c). It means that the D$_A$ center has the C_{3v} symmetry about the [111] direction. On the other hand, the large-bias topographies of the D$_A$ center look darker than the normal surface in both polarities [see Figs. 2(b) and 2(d)]. Hence the D$_A$ center is likely to have a geometrically hollow structure. Later we will address further structural features of the D$_A$ center like the possible incorporation of B and/or C atoms as in the B-X center for which Jones *et al.* [13] proposed a B-C pair at the nearest-neighbor sites though questioned by others [11,30]. Nonetheless, we do not attempt to determine the complete structure of the D$_A$ center in this paper because it requires a great deal of systematic investigation far beyond the scope of this work; we leave it for future study.

Since the dI/dV spectrum of the D$_A$ center slightly deviates from that of the normal surface near the VBM [see Fig. 2(a)], we have measured it again across the VBM with finer spectral bin spacing as displayed in Fig. 3(a). The red and blue curves in the figure are probed at two different positions of the D$_A$ center marked by red and blue crosses in Fig. 3(b), respectively. They have prominent peak structures at $+40$ mV, $+18$ mV, and -18 mV, which are termed as A_1, A_2, and A_3, respectively, in Fig. 3(a). We have also probed the squared wave functions of these shallow levels by using the scanning tunneling spectroscopy (STS) technique and displayed
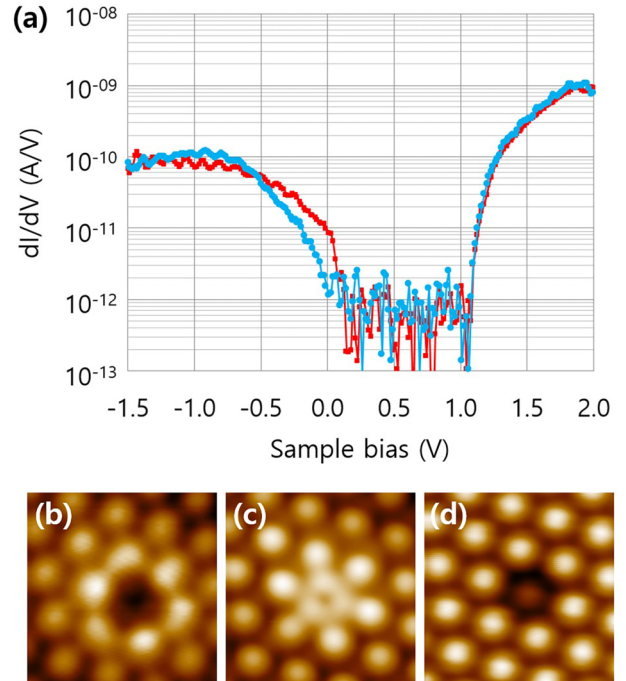
them in Figs. 3(c)–3(e), which reveal that the A_1, A_2, and A_3 levels are bounded with finite spatial extents. As a bound state accommodating a hole carrier, A_1 is the ground state located at -40 meV below the Fermi level (E_F) and A_2 and A_3 are the excited ones located at -18 meV and $+18$ meV, respectively, relative to E_F. The ground state (A_1) has similar binding energy as that of the B acceptor in Si, which suggests that the D$_A$ center is possibly a complex structure containing a B atom like the B-X center [12]. On the other hand, the lowest-lying excited state (A_2) is located above the ground one (A_1) by $\sim$22 meV. This value is almost identical to the nonhydrogenic transition energy ($\sim$23 meV) observed in the B-doped Si [7–10]. The latter has long been ascribed to the optical transition to the even-parity excited state ($1\Gamma_7^+$) of the B acceptor associated with the spin-orbit split-off band of Si [7,11]. But, unlike the $1\Gamma_7^+$ state, the squared wave function of the A_2 state shown in Fig. 3(d) has a nodelike line along the [$\bar{1}$10] direction and, therefore, it cannot be assigned to the even-parity $1\Gamma_7^+$ state. Recently, Pavlov *et al.* [3] suggested that the nonhydrogenic hole transition at $\sim$23 meV can be a dipole-allowed transition to the odd-parity excited state of the B-containing complex like the B-X center [12], not B itself, which has the C_{3v} symmetry about the [111] direction. The A_2 state that has a nodelike line and is probed in the threefold symmetric D$_A$ center looks more compatible with his argument. But, he assumes the modified hydrogenic levels proposed by Scott and Jones [12], which have energy-shifted s-like states and little-shifted p-like ones due to the different penetration to the atomic core of the complex structure (B-
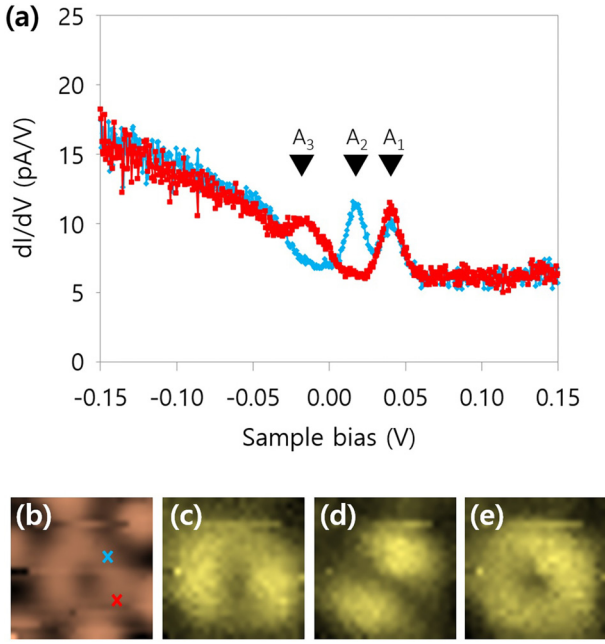
FIG. 3. (a) Red (blue) curve is the dI/dV spectrum measured at the red (blue) cross in (b) with the bin spacing of 0.6 mV. Three peak structures at +40 mV, +18 mV, and −18 mV are labeled as A_1, A_2, and A_3, respectively. (b) Topography of the D_A center probed with $V_{sample} = -0.2$ V and $I_t = 1.0$ nA. Its lateral dimension is 1.2×1.2 nm^2. (c)–(e) dI/dV maps or squared wave functions of A_3, A_2, and A_1 levels in (a), respectively, which are probed in the same region as that in (b). The tip-to-sample separation at each pixel of these maps is determined by the feedback loop to yield the tunneling current of $I_t = 1.0$ nA at the sample bias of $V_{sample} = -0.2$ V.

X center). This hydrogenic model, though modified, is still inconsistent with the energy spacings between A_1, A_2, and A_3 levels. We, therefore, ascribe them to a different origin, i.e., strain-driven mechanism as elaborated on below.

The wave function of the shallow acceptor state can be written as

$$\psi(\mathbf{r}) = \sum_t F_t(\mathbf{r})\phi_t(\mathbf{r}), \qquad (1)$$

where $\phi_t(\mathbf{r})$ are the Bloch functions at the zone center or Γ point of the unperturbed Si and the index t runs over (nearly) degenerate states at that point [31,32]. The slowly varying envelope functions $F_t(\mathbf{r})$ satisfy the Luttinger-Kohn Hamiltonian (H_{LK}) [31]:

$$\sum_{t'} [D_{tt'}^{\alpha\beta}(-i\nabla_\alpha)(-i\nabla_\beta) + U(\mathbf{r})\delta_{tt'}]F_{t'}(\mathbf{r}) = \varepsilon F_t(\mathbf{r}), \qquad (2)$$

where the numbers $D_{tt'}^{\alpha\beta}$ are related to the effective masses of hole carriers, whose specific forms are given in Ref. [31]. The perturbing potential $U(\mathbf{r})$ is due to the electric charge of the D_A center and is assumed to have the $-e^2/\kappa r$ form in this calculation, which would yield the hydrogenic energy levels. For the 1s level, Eq. (1) is simplified as

$$\psi(\mathbf{r}) = F_0(r)\overline{\phi}_t(\mathbf{r}), \qquad (3)$$

where $F_0(r)$ is the spherically symmetric envelope function and $\overline{\phi}_t$ are the Bloch functions at the Γ point

appropriate for the external perturbation if any [32,33]. The acceptor wave function in Eq. (3) transforms like the Bloch function and, therefore, the former would have the same point symmetry as the latter in the 1s level. For the unperturbed Si, there are six nearly degenerate Bloch functions at the VBM which are called the heavy-hole ($|3/2, \pm 3/2\rangle$), the light-hole ($|3/2, \pm 1/2\rangle$), and the spin-orbit split-off ($|1/2, \pm 1/2\rangle$) states. This valence band structure, however, is modified near the D_A center because it generates the strain fields around it. Such modification can be assessed by using the Bir-Pikus Hamiltonian (H_{BP}) [34] that reads in the $\{|j, m\rangle \,|\, j = \frac{3}{2}, \frac{1}{2}; \, m = \pm\frac{3}{2}, \pm\frac{1}{2}\}$ basis as

$$\begin{pmatrix} P+Q & -S & R & 0 & -\frac{1}{\sqrt{2}}S & \sqrt{2}R \\ -S^\dagger & P-Q & 0 & R & -\sqrt{2}Q & \sqrt{\frac{3}{2}}S \\ R^\dagger & 0 & P-Q & S & \sqrt{\frac{3}{2}}S^\dagger & \sqrt{2}Q \\ 0 & R^\dagger & S^\dagger & P+Q & -\sqrt{2}R^\dagger & -\frac{1}{\sqrt{2}}S^\dagger \\ -\frac{1}{\sqrt{2}}S^\dagger & -\sqrt{2}Q & \sqrt{\frac{3}{2}}S & -\sqrt{2}R & P+\Delta & 0 \\ \sqrt{2}R^\dagger & \sqrt{\frac{3}{2}}S^\dagger & \sqrt{2}Q & -\frac{1}{\sqrt{2}}S & 0 & P+\Delta \end{pmatrix}$$

$$(4)$$

for the hole carriers, where

$$P = -a_v(\epsilon_{xx} + \epsilon_{yy} + \epsilon_{zz}),$$

$$Q = -\frac{1}{2}b(\epsilon_{xx} + \epsilon_{yy} - 2\epsilon_{zz}),$$

$$R = \frac{\sqrt{3}}{2}b(\epsilon_{xx} - \epsilon_{yy}) - id\epsilon_{xy},$$

$$S = -d(\epsilon_{zx} - i\epsilon_{yz}), \qquad (5)$$

and Δ is the effective spin-orbit split-off energy [34,35]. Also, ϵ_{ij} is the symmetric strain tensor and a_v, b, and d are Bir-Pikus deformation potentials whose values for Si are 2.4 eV, −2.1 eV, and −5.1 eV, respectively [36].

The strain Hamiltonian H_{BP} has three doubly degenerate levels in general because it does not break the time-reversal symmetry. We denote them as $\{\phi_1^{(i)}, \phi_2^{(i)}\}$ for the E_i level with $i = 1$, 2, and 3. These states and levels turn out to match the experimentally probed ones in Fig. 3. To be specific, H_{BP} in Eq. (4) with $\Delta = 27.9$ meV, $P - (VBM - E_F) = 22.6$ meV, $Q = 11.1$ meV, $R = 8.7$ meV, and $S = 0.0$ meV has the same energies as the A_1, A_2, and A_3 levels within the error of ±0.1 meV, that is, $E_1 = -40$ meV, $E_2 = -18$ meV, and $E_3 = +18$ meV relative to E_F (see Supplemental Material [37]). Also, the squared wave functions $|\phi^{(i)}|^2$ of the E_i level ($i = 1, 2, 3$), which are computed with $|j, m\rangle$ or, equivalently, p_x, p_y, p_z orbitals at the bright positions in Fig. 4(a), are displayed in Figs. 4(b)–4(d) (see Supplemental Material [37]). Despite the slight mismatch, they resemble most features of the experimentally probed ones in Figs. 3(c)–3(e): the E_1 state has the threefold symmetry about the [111] direction with no nodal line as does the A_1 state, whereas E_2 and E_3 have the reduced symmetries with nodelike lines as do A_2 and A_3. Indeed, various sets of Δ, $P - (VBM - E_F)$, Q, and R values, e.g., those in Fig. 4(e), make the strain Hamiltonian H_{BP}
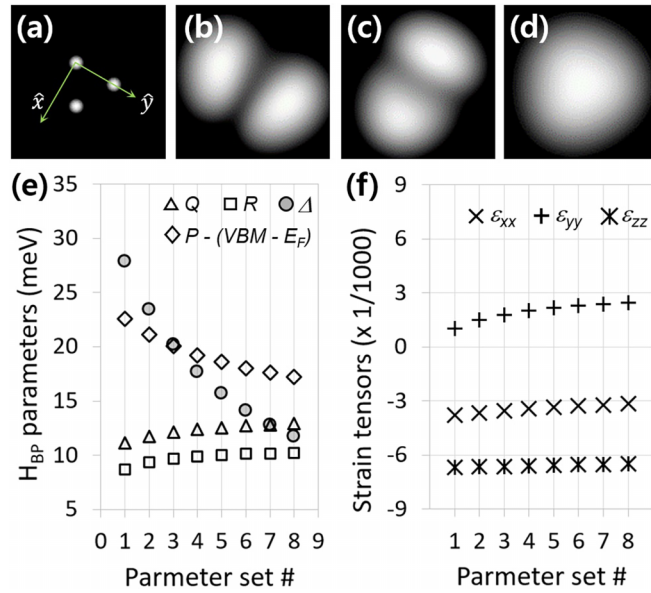
FIG. 4. (a) Positions of the ball-like features in Fig. 2(c) whose spacing is 3.84 Å. $\hat{z}$ is set to the surface normal, i.e., [111] direction and $\hat{x}$ ($\hat{y}$) to the [$11\bar{2}$] ([$\bar{1}10$]) direction. (b)–(d) Squared wave functions of E_3, E_2, and E_1 levels of H_{BP}, respectively. They are calculated with $\Delta = 27.9$ meV, $P - (VBM - E_F) = 22.6$ meV, $Q = 11.1$ meV, $R = 8.7$ meV, and $S = 0.0$ meV, as well as with $|j, m\rangle$ or, equivalently, p_x, p_y, p_z orbitals at the bright positions in (a). (e) Various sets of Δ, $P - (VBM - E_F)$, Q, and R parameters with which H_{BP} has $E_1 = -40$ meV, $E_2 = -18$ meV, and $E_3 = 18$ meV relative to E_F, and $|\phi^{(i)}|^2$'s similar to those in (b) to (d). For each parameter set, S is fixed to zero. (f) Strain tensors computed with Eq. (5) and the parameter values in (e). Here E_F is assumed to be at the *VBM*.

reproduce the experimentally probed energies and squared wave functions with good qualities. Noteworthy is that the spin-orbit energy Δ in Fig. 4(e) is significantly smaller than that (i.e., 44 meV) of the unperturbed Si regardless of its large variation. It suggests that the D_A center contains in its local structure other species like, e.g., carbon (C), which has smaller spin-orbit splitting ($\Delta \sim 13$ meV for C) [40] than Si but, as mentioned above, we leave it for future study to uncover the detailed structure of the D_A center. The strain tensors in Eq. (5) can also be evaluated from the parameter values in Fig. 4(e) (see Supplemental Material [37]). The

results for ϵ_{xx}, ϵ_{yy}, and ϵ_{zz} are displayed in Fig. 4(f) with $\epsilon_{xy} = \epsilon_{yz} = \epsilon_{zx} = 0.0$: the formers are determined within the constant error of $\frac{1}{3a_v}(VBM - E_F)$, whose magnitude is as large as $\pm 3.5 \times 10^{-3}$ because of the uncertainty (i.e., ± 25 meV) of the E_F position relative to the VBM in our heavily B-doped Si sample [see the blue curve in Fig. 2(a)]. The strain values in Fig. 4(f) (with an additive constant) indicate that the D_A center is subject to the anisotropic strain fields in both in-plane and out-of-plane directions. Such anisotropic strain fields generally cause the mixing of the heavy/light hole states with the spin-orbit split-off one (see Supplemental Material [37]) and yield new Bloch states with the reduced symmetries like A_2 and A_3 [see Figs. 3(d) and 3(c)] [41,42]. In other words, the A_1, A_2, and A_3 states of the D_A center develop as a consequence of the strain-induced mixing of the valence bands at the Γ point. This strain-driven mechanism contrasts the hydrogenic model for the B-X center proposed by Scott and Jones [12] and referred by Pavlov *et al.* [3], as well as the even-parity excited state ($1\Gamma_7^+$) of the B acceptor suggested by Wright and Moonradian [7], providing another origin for the nonhydrogenic hole transition at ~ 23 meV in the B-doped Si.

IV. CONCLUSION

In conclusion, the D_A center with the C_{3v} symmetry about the [111] direction is produced on the (111) surface of the heavily B-doped Si during the thermal annealing process though its internal structure is not uncovered yet. It develops three acceptor levels at -40 meV, -18 meV, and $+18$ meV relative to E_F as a consequence of the strain-induced mixing of the valence bands near the D_A center, whose spacing between the ground state with threefold symmetry and the lowest-lying excited state with a nodelike line is ~ 22 meV. Thus it provides a strain-driven mechanism for the nonhydrogenic hole transition in the B-doped Si [7–10], though it does not necessarily deny other mechanisms like the modified hydrogenic levels for the B-X center [3,12] or the $1\Gamma_7^+$ state of the B acceptor in Si [7].

[1] J. Salfi, J. A. Mol, D. Culcer, and S. Rogge, Charge-insensitive single-atom spin-orbit qubit in silicon, Phys. Rev. Lett. **116**, 246801 (2016).

[2] S. Zhang, Y. He, and P. Huang, Acceptor-based qubit in silicon with tunable strain, Phys. Rev. B **107**, 155301 (2023).

[3] S. G. Pavlov, N. Deßmann, V. N. Shastin, R. Kh. Zhukavin, B. Redlich, A. F. G. van der Meer, M. Mittendorff, S. Winnerl, N. V. Abrosimov, H. Riemann, and H.-W. Hübers, Terahertz stimulated emission from silicon doped by hydrogenlike acceptors, Phys. Rev. X **4**, 021009 (2014).

[4] S. A. Lynch, P. Townsend, G. Matmon, D. J. Paul, M. Bain, H. S. Gamble, J. Zhang, Z. Ikonic, R. W. Kelsall, and P. Harrison, Temperature dependence of terahertz optical transitions from boron and phosphorus dopant impurities in silicon, Appl. Phys. Lett. **87**, 101114 (2005).

[5] C. Kittel, *Introduction to Solid State Physics*, 6th ed. (Wiley, Singapore, 1991).

[6] R. Buczko and F. Bassani, Shallow acceptor resonant states in Si and Ge, Phys. Rev. B **45**, 5838 (1992).

[7] G. B. Wright and A. Mooradian, Raman scattering from donor and acceptor impurities in silicon, Phys. Rev. Lett. **18**, 608 (1967).

[8] J. M. Cherlow, R. L. Aggarwal, and B. Lax, Raman scattering and photoluminescence in boron-doped and arsenic-doped silicon, Phys. Rev. B **7**, 4547 (1973).

[9] J. Serrano, A. Wysmolek, T. Ruf, and M. Cardona, Spin-orbit splitting of acceptor states in Si and C, Phys. B: Condens. Matter **273-274**, 640 (1999).

[10] H. R. Chandrasekhar, A. K. Ramdas, and S. Rodriguez, Stress-induced mixing of the spin-orbit-split acceptor states of silicon, Phys. Rev. B **12**, 5780 (1975).

[11] K. J. Morse, R. J. S. Abraham, D. P. Franke, N. V. Abrosimov, and M. L. W. Thewalt, Even-parity excited states of the acceptor boron in silicon revisited, Phys. Rev. B **93**, 125207 (2016).

[12] W. Scott and C. E. Jones, Infrared spectra of new acceptor levels in boron-doped and gallium-doped silicon, J. Appl. Phys. **50**, 7258 (1979).

[13] C. E. Jones, D. Schafer, W. Scott, and R. J. Hager, Carbon-acceptor pair centers (X centers) in silicon, J. Appl. Phys. **52**, 5148 (1981).

[14] G. Mahieu, B. Grandidier, D. Deresmes, J. P. Nys, D. Stiévenard, and Ph. Ebert, Direct evidence for shallow acceptor states with nonspherical symmetry in GaAs, Phys. Rev. Lett. **94**, 026407 (2005).

[15] S. Loth, M. Wenderoth, L. Winking, R. G. Ulbrich, S. Malzer, and G. H. Döhler, Probing semiconductor gap states with resonant tunneling, Phys. Rev. Lett. **96**, 066403 (2006).

[16] F. Marczinowski, J. Wiebe, J.-M. Tang, M. E. Flatté, F. Meier, M. Morgenstern, and R. Wiesendanger, Local electronic structure near Mn acceptors in InAs: Surface-induced symmetry breaking and coupling to host states, Phys. Rev. Lett. **99**, 157202 (2007).

[17] J.-M. Jancu, J.-C. Girard, M. O. Nestoklon, A. Lemaître, F. Glas, Z. Z. Wang, and P. Voisin, STM images of subsurface Mn atoms in GaAs: Evidence of hybridization of surface and impurity states, Phys. Rev. Lett. **101**, 196801 (2008).

[18] C. Çelebi, J. K. Garleff, A. Yu. Silov, A. M. Yakunin, P. M. Koenraad, W. Van Roy, J.-M. Tang, and M. E. Flatté, Surface induced asymmetry of acceptor wave functions, Phys. Rev. Lett. **104**, 086404 (2010).

[19] P. M. Koenraad and M. E. Flatté, Single dopants in semiconductors, Nat. Mater. **10**, 91 (2011).

[20] W. H. Press and S. A. Teukolsky, Savitzky-Golay smoothing filters, Comput. Phys. **4**, 669 (1990).

[21] D. Eom, C.-Y. Moon, and J.-Y. Koo, Switching the charge state of individual surface atoms at Si(111)-$\sqrt{3} \times \sqrt{3}$:B Surfaces, Nano Lett. **15**, 398 (2015).

[22] I.-W. Lyo, E. Kaxiras, and P. Avouris, Adsorption of boron on Si(111): Its effect on surface electronic states and reconstruction, Phys. Rev. Lett. **63**, 1261 (1989).

[23] R. L. Headrick, I. K. Robinson, E. Vlieg, and L. C. Feldman, Structure determination of the Si(111) : B($\sqrt{3} \times \sqrt{3}$)$R30°$ surface: Subsurface substitutional doping, Phys. Rev. Lett. **63**, 1253 (1989).

[24] P. Bedrossian, D. M. Chen, K. Mortensen, and J. A. Golovchenko, Demonstration of the tunnel-diode effect on an atomic scale, Nature (London) **342**, 258 (1989).

[25] M. Berthe, R. Stiufiuc, B. Grandidier, D. Deresmes, C. Delerue, and D. Stiévenard, Probing the carrier capture rate of a single quantum level, Science **319**, 436 (2008).

[26] T. H. Nguyen, G. Mahieu, M. Berthe, B. Grandidier, C. Delerue, D. Stiévenard, and P. Ebert, Coulomb energy determination of a single Si dangling bond, Phys. Rev. Lett. **105**, 226404 (2010).

[27] D. Eom, C.-Y. Moon, and J.-Y. Koo, Determining the Jahn-Teller stabilization energy of adatom vacancies on a Si(111)-$\sqrt{3} \times \sqrt{3}$:B surface, Phys. Rev. B **100**, 115302 (2019).

[28] E. Kaxiras, K. C. Pandey, F. J. Himpsel, and R. M. Tromp, Electronic states due to surface doping: Si(111)$\sqrt{3} \times \sqrt{3}$B, Phys. Rev. B **41**, 1262(R) (1990).

[29] T. M. Grehk, P. Mårtensson, and J. M. Nicholls, Occupied and unoccupied surface states on the Si(111)$\sqrt{3} \times \sqrt{3}$:B surface, Phys. Rev. B **46**, 2357 (1992).

[30] J. J. Rome, W. C. Mitchel, G. J. Brown, D. W. Fischer, M. C. Ohmer, and T. L. Peterson, X-center formation by neutron irradiation of Ga-doped float-zone silicon, Appl. Phys. Lett. **41**, 254 (1982).

[31] J. M. Luttinger and W. Kohn, Motion of electrons and holes in perturbed periodic fields, Phys. Rev. **97**, 869 (1955).

[32] D. Schechter, Theory of shallow acceptor states in Si and Ge, J. Phys. Chem. Solids **23**, 237 (1962).

[33] G. L. Bir, Jahn-Teller effect on impurity centers in semiconductors, Sov. Phys. JETP **24**, 372 (1967).

[34] G. L. Bir and G. E. Pikus, *Symmetry and Strain-Induced Effects in Semiconductors* (Wiley, New York, 1974).

[35] C. Y.-P. Chao and S. L. Chuang, Spin-orbit-coupling effects on the valence-band structure of strained semiconductor quantum wells, Phys. Rev. B **46**, 4110 (1992).

[36] J.-C. Merle, M. Capizzi, P. Fiorini, and A. Frova, Uniaxially stressed silicon: Fine structure of the exciton and deformation potentials, Phys. Rev. B **17**, 4821 (1978).

[37] See Supplemental Material at http://link.aps.org/supplemental/10.1103/PhysRevB.108.235304 for the detailed calculations of the Bir-Pikus Hamiltonian, the squared wave functions, the strain tensors, and the valence band mixing ratios, which includes Refs. [34–36,38,39].

[38] M. Lax and E. Burstein, Broadening of impurity levels in silicon, Phys. Rev. **100**, 592 (1955).

[39] L. Viña and M. Cardona, Effect of heavy doping on the optical properties and the band structure of silicon, Phys. Rev. B **29**, 6739 (1984).

[40] P. Carrier and S.-H. Wei, Calculated spin-orbit splitting of all diamondlike and zinc-blende semiconductors: Effects of $p_{1/2}$ local orbitals and chemical trends, Phys. Rev. B **70**, 035212 (2004).

[41] Y. Léger, L. Besombes, L. Maingault, and H. Mariette, Valence-band mixing in neutral, charged, and Mn-doped self-assembled quantum dots, Phys. Rev. B **76**, 045331 (2007).

[42] A. V. Koudinov, I. A. Akimov, Y. G. Kusrayev, and F. Henneberger, Optical and magnetic anisotropies of the hole states in Stranski-Krastanov quantum dots, Phys. Rev. B **70**, 241305(R) (2004).